ChemComm

COMMUNICATION

View Article Online
View Journal | View Issue

Cite this: *Chem. Commun.*, 2019, 55, 4031

Received 31st January 2019,
Accepted 8th March 2019

DOI: 10.1039/c9cc00733d

rsc.li/chemcomm

Performance enhancement of $AgBi_2I_7$ solar cells by modulating a solvent-mediated adduct and tuning remnant BiI_3 in one-step crystallization†

Ashish Kulkarni,* Ajay K. Jena, Masashi Ikegami and Tsutomu Miyasaka*

We modulated a solvent-mediated adduct for one-step crystallization of lead-free $AgBi_2I_7$ at a lower temperature (90 °C) and to obtain remnant BiI_3 by controlling the nature of the substrate and precursor concentration. This eventually resulted in remarkable enhancement in the power conversion efficiency, reaching 2.12%, and the long-term stability of $AgBi_2I_7$ solar cells towards light, heat and humidity.

The power conversion efficiency (PCE) of hybrid perovskite solar cells has skyrocketed to more than 23% in just 10 years.[1–3] Such a steep rise in PCE is credited to the exceptional optoelectronic properties of perovskites and simple solution fabrication processes.[4–8] Despite such advantages, lead perovskites suffer from long-term stability[9] and Pb-toxicity.[10] Although the amount of Pb used in photovoltaic devices is not high,[11] it is believed that the presence of Pb can stand as a major obstacle in the way to commercialization of perovskite solar cells.[10] To address this toxicity issue of Pb, perovskite materials based on tin (Sn)[12] and germanium (Ge)[13] have been explored but the poor performance and instability of these devices under ambient atmosphere due to disproportionation or oxidation of Sn^{2+} and Ge^{2+} have been little discouraging.[14]

Due to the isoelectronic ($6s^2$) nature of the bismuth (Bi^{3+}) cation, it has also been employed as a non-toxic alternative to Pb^{2+}.[15,16] Lower dimensional $A_3Bi_2I_9$ (A = MA^+ and Cs^+) and Bi-based double perovskites have been explored as photovoltaic candidates. However, the low electronic and structural dimensionality in the former case and the low charge carrier mobility in the latter one have so far limited the PCE.[17–19] Moreover, their indirect wide band gap (>2.2 eV) limits their light-harvesting properties. Therefore, several three-dimensional silver (Ag^+) iodobismuthate based light absorbing materials such as $AgBi_2I_7$ have attracted recent attention due to their favourable optoelectronic properties for photovoltaic applications. Additionally, direct and lower bandgaps (1.85–1.9 eV) of $AgBi_2I_7$, compared to those of bismuth based hybrid perovskites, enable improved light harvesting properties in the former case.

In the very first study, Kim *et al.* reported $AgBi_2I_7$ based solar cells with a PCE of 1.2%.[20] However, this efficiency was not reproduced in the follow-up studies by Johansson *et al.*[21] and Shao *et al.*[22,23] who demonstrated a PCE of 0.4% and 0.52% respectively for the same $AgBi_2I_7$ solar cells. Such a poor reproducibility can be due to the sensitivity of $AgBi_2I_7$ to the annealing temperature, which, although has not been investigated thoroughly, was indicative from the studies of Kim *et al.*,[20] Johansson *et al.*[21] and Mitzi *et al.*[24] While Kim *et al.*[20] and Johansson *et al.*[21] reported the crystallization of $AgBi_2I_7$ at a relatively high temperature (150 °C) due to a strong solvent-intermediate adduct of BiI_3 and AgI with *n*-butylamine as the solvent, Mitzi *et al.*[24] recently reported that annealing the $AgBi_2I_7$ thin film at the same temperature (150 °C) results in loss of BiI_3 leading to the formation of $Ag_{1.16}Bi_{1.04}I_{4.00}$ instead of $AgBi_2I_7$. Thus, overcoming this phase impurity issue and obtaining the $AgBi_2I_7$ thin film at a low-temperature (90–100 °C) becomes vitally important for further enhancement in performance and reproducibility.

In the present study, we employ dimethyl sulfoxide (DMSO) as a solvent to obtain a $AgBi_2I_7$ thin film at a relatively low-temperature (90 °C) (due to a weak solvent-mediated adduct) and compare it with previously reported *n*-butylamine which forms strong solvent-mediated adducts. The influence of strong and weak solvent intermediate adducts, formed respectively with *n*-butylamine and DMSO solvents, on the crystallization, crystal orientation and optoelectronic properties of $AgBi_2I_7$ films has been studied. In addition, we show the importance of remnant BiI_3, which interestingly appears in the DMSO case (only for 20 wt%) and is believed to play a crucial role in enhancing the charge transport, performance, and stability of $AgBi_2I_7$ solar cells. As a result, the best device demonstrated a PCE of 2.12% (average PCE = 1.8%) with high stability under continuous 1 sun illumination (100 mW cm^{-2}) (operated at a maximum power point for 1 h) and upon exposure (un-encapsulated cells) to 50–60% relative humidity for 75 days and heat stress (100 °C for 5 h).

Graduate School of Engineering, Toin University of Yokohama, 1614 Kurogane-cho, Aoba, Yokohama, Kanagawa 225-8503, Japan.
E-mail: ashish.kulkarni786@gmail.com, miyasaka@toin.ac.jp

† Electronic supplementary information (ESI) available: Experimental procedure, light intensity dependent studies, XRD, top surface SEM, *J–V* characteristic curves, histogram, box plot and tables. See DOI: 10.1039/c9cc00733d

The study reveals an important correlation between the solvated intermediate adducts and crystallization process, which strongly influences the device performance and long-term stability of lead-free eco-friendly $AgBi_2I_7$ solar cells.

Kim *et al.*[20] and Johansson *et al.*[21] employed *n*-butylamine to dissolve the mixture of 20 wt% AgI and BiI_3 (to form $AgBi_2I_7$) because, as they mentioned, AgI was not soluble in polar aprotic solvents such as DMF and/or DMSO.[20,21] However, we found that the mixture of AgI and BiI_3 can get dissolved in DMSO upon constant stirring at 70 °C for 30 min (Fig. S1, ESI†). As DMSO is a well-known two-electron donor (Lewis base) ligand and BiI_3 is reported to form adducts or coordination complexes with a range of Lewis base ligands, we believe that the BiI_3–DMSO adduct or $[BiI_{3+x}]^{x-}$ complex ions[25] that are formed in the solvent probably helps in the dissolution of AgI in DMSO (as AgI is not independently soluble in DMSO). The optical absorption spectra (Fig. 1a) of the $AgBi_2I_7$ film (from the solution in *n*-butylamine) at different annealing temperatures, as obtained by UV-vis spectroscopy, display that the as-prepared film (before the heating step) shows a sharp absorption band at 475 nm which essentially corresponds to the bismuth iodide octahedral complex.[26,27] This absorption peak corresponding to the bismuth iodide octahedral complex appeared even after annealing the film at 120 °C. Therefore, heating at 150 °C and above was required for its complete removal from the spin-coated films. This can be due to the strong solvent intermediate adduct formed by both BiI_3 and AgI with *n*-butylamine.[20,21] On the other hand, the as-prepared $AgBi_2I_7$ thin film obtained from the solution made in DMSO showed an absorption band at around ~510 nm and ~440 nm (Fig. 1b) which is different from that of the *n*-butylamine case, evidencing the formation of different intermediate adducts. Moreover, decomposition of this intermediate adduct in DMSO occurred at a lower temperature (90 °C) in comparison to the *n*-butylamine case (150 °C), which was evident from the absorption spectra (~610 nm) (Fig. 1a and b). This clearly indicates that the BiI_3–DMSO–AgI solvent intermediate adduct is not as strong as BiI_3–*n*-butylamine–AgI. From this, it can also be inferred that the crystallization process of $AgBi_2I_7$ through the *n*-butylamine route differs from that of DMSO. An E_g of ~1.89 eV and ~1.78 eV was obtained for the $AgBi_2I_7$ thin film (obtained from both *n*-butylamine and DMSO cases) by assuming a direct and indirect bandgap (Fig. S2, ESI†), respectively.

The crystal structures of $AgBi_2I_7$ obtained from 20 wt% solutions in both the solvents were analysed by X-ray diffraction (XRD) and the results are shown in Fig. 2a. The diffraction pattern of $AgBi_2I_7$ obtained from the *n*-butylamine route exhibited major characteristic peaks at 2θ equal to 12°, 25°, 29°, and 42° corresponding to the (111), (311), (400) and (440) crystal planes, respectively, which is resolved in the $Fd3m$ space group.[20,21] The XRD pattern of $AgBi_2I_7$ obtained from the DMSO route also showed the same characteristic peaks except for a less intense doublet peak at $2\theta = 42°$ (Fig. 2a) (JCPDS card – PDF 00-034-1372) (Fig. S3, ESI†). Such a doublet peak at $2\theta = 42°$ has been observed previously by Johansson *et al.*[21] for Ag_2BiI_5. Hence, in order to verify this, we recorded the diffraction pattern of the Ag_2BiI_5 ($AgI : BiI_3 = 2:1$) thin film obtained from the solution in *n*-butylamine and compared it with $AgBi_2I_7$ diffraction peaks. As shown in Fig. S4a (ESI†), Ag_2BiI_5 obtained from the *n*-butylamine case showed a doublet peak at $2\theta = 42°$ (the XRD pattern for $AgBi_2I_5$ from DMSO was very weak for comparison). However, this doublet peak looked different from that of the $AgBi_2I_7$, as evidenced by a shift in the diffraction peaks (Fig. S4b, ESI†). This indicates that Ag_2BiI_5 as an impurity was not formed when 20 wt% BiI_3 and AgI were dissolved (to form $AgBi_2I_7$) in DMSO; however, this impurity could still be present and detailed investigation is required. In fact, this doublet peak, as confirmed from a comparison of $AgBi_2I_7$ and BiI_3 XRD patterns (Fig. 2b), consisted of one peak (~41.2°) from BiI_3 and the other (~42.2°) from the $AgBi_2I_7$ cubic phase, confirming the presence of remnant BiI_3 in the film.[23,27] Interestingly, the appearance of this remnant BiI_3 depended on the concentration of the precursor solution, that is, with an increase in the solution concentration to 40 and 60 wt%, the doublet peak disappeared and a single high intense peak corresponding to (440) appeared (Fig. S4c, ESI†). In addition to the solution concentration, the appearance of this remnant BiI_3 was also found to depend on the under-layer substrate. The solution of 20 wt% $AgBi_2I_7$ in DMSO, when deposited on an FTO/TiO_2 mesoporous layer, produced a doublet peak (with remnant BiI_3) (Fig. 2a and Fig. S4c, ESI†) but the same solution deposited on glass showed only one peak (corresponding to the (440) cubic phase of $AgBi_2I_7$) (Fig. S4e, ESI†), suggesting that the TiO_2 mesoporous layer affects the crystallization of $AgBi_2I_7$ to yield some remnant BiI_3. Although the exact reason for the appearance of remnant BiI_3 in this case (20 wt% $AgBi_2I_7$ thin film on the mesoporous TiO_2 layer), despite no excess BiI_3 being used in the starting mixture, is not clear at present, the result suffices its appearance when DMSO (which does not form the strong intermediate adduct) and precursor materials at low concentration are used. Unlike the DMSO case, butylamine (with 20 wt% $AgBi_2I_7$) did not favour the formation of BiI_3 most probably due to the strong intermediate adduct with both BiI_3 and AgI, and due to a different crystallization route. Detailed investigation, which is

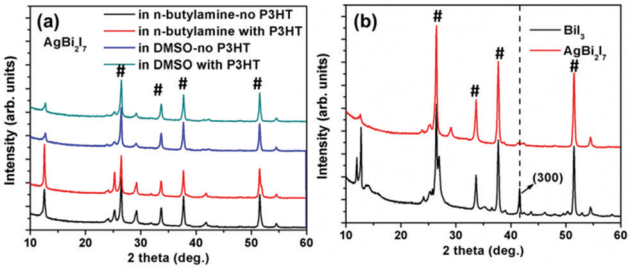

Fig. 2 The X-ray diffraction pattern of (a) $AgBi_2I_7$ obtained from *n*-butylamine and DMSO and (b) its comparison with the XRD pattern of BiI_3.

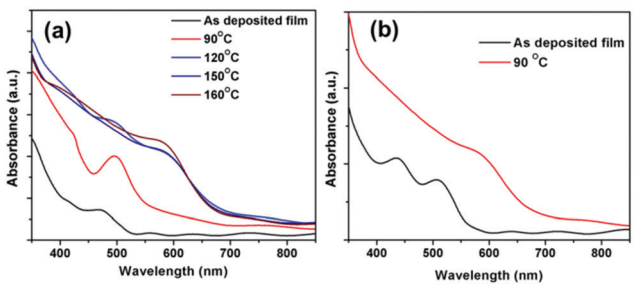

Fig. 1 The UV–vis absorption spectra of the $AgBi_2I_7$ thin film obtained at different temperatures from (a) *n*-butylamine and (b) DMSO.

in our plan for future studies, is required to understand how exactly the solvents, substrates and solution concentrations affect the crystallization of $AgBi_2I_7$ such that the composition of the final film is altered.

The effect of atmosphere on the $AgBi_2I_7$ thin film was investigated by measuring the XRD patterns of $AgBi_2I_7$ (obtained from both *n*-butylamine and DMSO) with and without the P3HT hole transport material (HTM) as an upper layer. In the *n*-butylamine case (Fig. 2a), we observed a reduction in the peak intensity of the $AgBi_2I_7$ film without the P3HT upper layer while the film with P3HT showed no change, indicating the sensitivity of $AgBi_2I_7$ to ambient atmosphere which is slightly protected by the P3HT upper layer.[21,28] In contrast, we observed no difference in the diffraction peak intensity of $AgBi_2I_7$ (with and without P3HT) obtained from the DMSO route (Fig. 2a), evidencing its enhanced stability towards ambient atmosphere. This indicates that the stability of $AgBi_2I_7$ is highly dependent on the crystallization process and its root lies in the choice of the precursor solvent and also it must be related to the intrinsic structural stability of the material, which depends strongly on the crystal quality and phase purity.

To check the effect of the solvent intermediate adduct on the morphology, $AgBi_2I_7$ solutions in *n*-butylamine and DMSO were spin-coated on mesoporous TiO_2-coated FTO substrates and micrograph analysis was performed using a scanning electron microscope (SEM). $AgBi_2I_7$ obtained from *n*-butylamine (Fig. 3a) showed large isolated spherical grains with a large area of exposed TiO_2 (also see Fig. S5, ESI†). The difference in morphology of the $AgBi_2I_7$ film in the present case from previous reports[20,21] can be due to the difference in processing conditions; the film fabrication in our case was performed in an ambient atmosphere and by anti-solvent drenching (see the Experimental section in the ESI†). Large grains with a non-uniform capping layer, making poor interfacial connections and allowing the contact of P3HT (HTM) and Au (metal electrode) with the mesoporous TiO_2 layer, could be seen from the cross-sectional view (Fig. 3b) of the device. On the other hand, $AgBi_2I_7$ obtained from solutions (20 and 40 wt%) in DMSO showed uniform grains without pinholes (Fig. 3c and Fig. S6, ESI†) and a thin uniform capping layer (Fig. 3d), forming a smooth interface with neighbouring charge transport layers. From the preceding results (XRD and SEM), it is evident that the solvent in the precursor solution plays a significant role in modulating the crystallization and morphology of $AgBi_2I_7$.

To study the effect of crystallization and appearance/disappearance of remnant BiI_3 on the photovoltaic performance, we fabricated devices with $AgBi_2I_7$, obtained from the *n*-butylamine and DMSO route, as an active layer sandwiched between mesoporous TiO_2 and pure P3HT (without dopants) as shown in Fig. S7a (ESI†). The current density (J)–voltage (V) characteristic plots are presented in Fig. 4. The best performing device with $AgBi_2I_7$ obtained from the *n*-butylamine route showed a short-circuit current density (J_{sc}) = 1.45 mA cm^{-2}, an open-circuit voltage (V_{oc}) = 0.52 V, and a fill factor (FF) = 0.43, resulting in a PCE = 0.33%. The obtained PCE is in agreement with the reports by Johansson *et al.*[21] and Shao *et al.*[22,23] and contrasts the first report by Kim *et al.*[20] In contrast, when the precursor solvent was changed to DMSO, the performance of the cells improved dramatically with the best device showing J_{sc} = 4.83 mA cm^{-2}, V_{oc} = 0.62 V, FF = 0.70 and PCE = 2.12% (Fig. 4a) with negligible hysteresis and high reproducibility (Fig. S7b and c, ESI†). The statistic plot (Fig. S8a–d, ESI†) of device parameters obtained from 40 devices of each kind shows significant augmentation in J_{sc} and FF with a slight increment in V_{oc} when DMSO was chosen as the precursor solvent. It is to be noted that the obtained J_{sc} and PCE are one of the highest values ever reported for $AgBi_2I_7$ based solar cells (also see Table S1, ESI†) using P3HT as HTM. Enhancement in J_{sc}, in this case, was expected to be due to the greater coverage and uniform film (Fig. 3c). However, based on a comparison of this result with that of the films made from 40 wt% solution in DMSO (Fig. 3c and Fig. S6, ESI†), it was rather indicative that not the film coverage or morphology but the remnant BiI_3 in the 20 wt% case (not seen in higher concentration cases) (Fig. 2b, Fig. S4c and d, ESI†) is

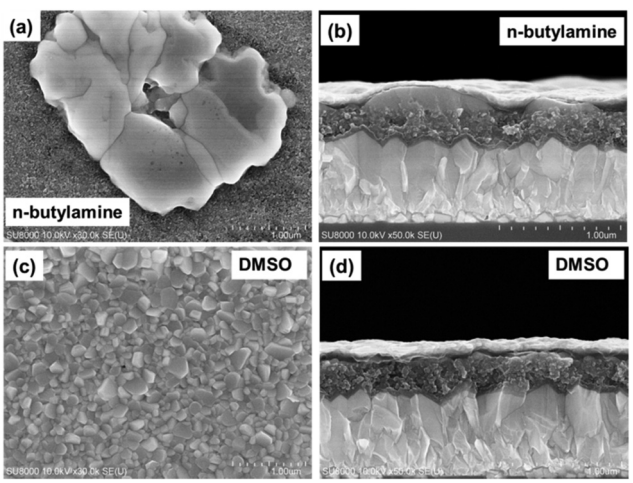

Fig. 3 The top and cross-sectional SEM image of $AgBi_2I_7$ obtained from (a and b) *n*-butylamine and (c and d) DMSO.

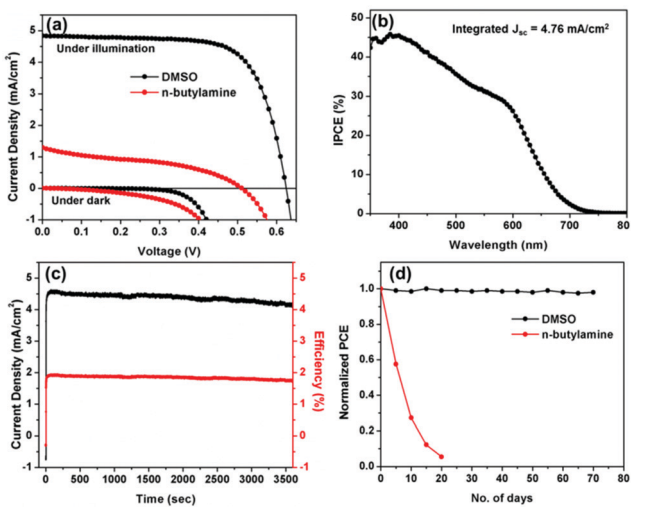

Fig. 4 (a) The current density–voltage (J–V) characteristic curve of the best performing devices, (b) the IPCE spectrum of $AgBi_2I_7$ device obtained from the DMSO-solvent route, (c) steady-state current density and efficiency at a maximum power point under continuous 1 sun illumination (100 mW cm^{-2}), and (d) normalized efficiency plot of devices (non-encapsulated) showing stability upon exposure to ambient 50–60% relative humidity.

responsible for the improvement of J_{sc} and device performance. Even though the films made from higher wt% solution in DMSO had a similar uniformity, coverage and morphology, the J_{sc} and overall performance dropped significantly (Fig. S9 and Table S2, ESI†). Therefore, remnant BiI_3 possibly helps in transporting the photo-generated carriers[27,29] into the neighbouring charge transport layers, resulting in the enhancement of J_{sc} and thus PCE. Fig. 4b depicts the incident photon to current conversion efficiency (IPCE) plot of the best performing $AgBi_2I_7$ solar cell covering the visible region with a sharp absorption onset at around ~740 nm. J_{sc} equivalent to 4.76 mA cm^{-2} was obtained by integrating the IPCE spectra, which matches well with the J_{sc} value (4.83 mA cm^{-2}) obtained from the *J–V* measurement. To understand the recombination losses in the cell, we also performed light intensity dependent measurements of the best performing devices and the results are discussed in the ESI† (explanation S1) and shown in Fig. S10.

Furthermore, we performed a stability test of the best performing $AgBi_2I_7$ devices and Fig. 4c shows the time course of steady-state photocurrent and efficiency at a maximum power point under continuous 1 sun (100 mW cm^{-2}) illumination for 1 h. The best performing non-encapsulated device shows good stability with a steady-state efficiency of 1.89%. We have also performed a long-term stability test by exposing the non-encapsulated $AgBi_2I_7$ devices obtained from DMSO and *n*-butylamine solvents to ambient air with a relative humidity of 50–60%. As can be seen in the normalized efficiency plot (Fig. 4d), the device with $AgBi_2I_7$ obtained from the *n*-butylamine solution degraded rapidly upon exposure to a humid atmosphere and is in line with the observation made in the XRD pattern of the $AgBi_2I_7$ thin film (Fig. 2a) while for the device with films made from the DMSO solution, the efficiency lasted up to 75 days without almost no change. Additionally, $AgBi_2I_7$ thin films were quite stable towards heat stress (100 °C) (Fig. S11, ESI†) for 5 h. The high stability of $AgBi_2I_7$ devices (obtained from DMSO) towards continuous illumination and exposure to humidity implies the greater material stability of $AgBi_2I_7$, which can be attributed to the intrinsic structural stability (as it is processed at low temperature) and the presence of remnant BiI_3.

In summary, a solvent engineering technique was employed to tune the crystallization route to obtain a $AgBi_2I_7$ thin film at a relatively low temperature. In contrast to the *n*-butylamine case, a uniform, pin-hole free layer was obtained when lower and higher concentration solutions of $AgBi_2I_7$ in DMSO were used for deposition. Interestingly, remnant BiI_3 appeared when a lower concentration of precursor materials was dissolved in DMSO, contrasting the *n*-butylamine case. As a result, the device demonstrated a best PCE of 2.12% (average 1.8%) with the use of non-doped P3HT (HTM). Enhancement of efficiency we believe is enabled by the presence of remnant BiI_3. Moreover, the devices showed enhanced stability under continuous illumination, towards ambient ~50–60% humidity and 100 °C heat stress. A further gain in performance of the system can be accompanied by understanding the crystallization process and the appearance of remnant BiI_3 and its role in efficiency enhancement, as well as *via* exploring suitable solvents and charge transport layers.

A. K. would like to acknowledge the Japan Society for the Promotion of Science (JSPS) for the JSPS postdoctoral fellowship. T. M. acknowledges financial support from the JSPS Grant-in-Aid for Scientific research B Grant No. 26289265 and the New Energy and Industrial Development Organization (NEDO).

Conflicts of interest

There are no conflicts to declare.

Notes and references

1 A. Kojima, K. Teshima, Y. Shirai and T. Miyasaka, *J. Am. Chem. Soc.*, 2009, **131**, 6050.
2 L. Meng, C. Sun, R. Wang, W. Huang, Z. Zhao, P. Sun, T. Huang, J. Xue, J.-W. Lee, C. Zhu, Y. Huang, Y. Li and Y. Yang, *J. Am. Chem. Soc.*, 2018, **140**(49), 17255.
3 Best solar cell efficiency chart, https://www.nrel.gov/pv/assets/pdfs/pv-efficiencies-07-17-2018.pdf, accessed on 22nd January 2019.
4 T. Miyasaka, *Chem. Lett.*, 2015, **44**, 720.
5 S. D. Stranks, G. E. Eperon, G. Grancini, C. Menelaou, M. J. P. Alcocer, T. Leijtens, L. M. Herz, A. Petrozza and H. J. Snaith, *Science*, 2013, **342**, 341.
6 G. C. Xing, N. Mathews, S. Y. Sun, S. S. Lim, Y. M. Lam, M. Graetzel, S. Mhaisalkar and T. C. Sum, *Science*, 2015, **342**, 344.
7 J. You, Z. Hong, Y. Yang, Q. Chen, M. Cai, T.-B. Song, C.-C. Chen, S. Lu, Y. Liu, H. Zhou and Y. Yang, *ACS Nano*, 2014, **8**(2), 1674.
8 A. Kulkarni, A. K. Jena, H.-W. Chen, Y. Sanehira, M. Ikegami and T. Miyasaka, *Sol. Energy*, 2016, **136**, 379.
9 B. Chaudhary, A. Kulkarni, A. K. Jena, M. Ikegami, Y. Udagawa, H. Kunugita, K. Ema and T. Miyasaka, *ChemSusChem*, 2017, **10**(11), 2473.
10 A. Babayigit, A. Ethirajan, M. Muller and B. Conings, *Nat. Mater.*, 2016, **15**, 247–251.
11 N.-G. Park, M. Graetzel, T. Miyasaka, K. Zhu and K. Emery, *Nat. Energy*, 2016, **1**, 16152.
12 M. Konstantakou and T. Stergiopoulos, *J. Mater. Chem. A*, 2017, **5**, 11518.
13 I. Kopacic, B. Friesenbichler, S. F. Hoefler, B. Kunert, H. Plank, T. Rath and G. Trimmel, *ACS Appl. Energy Mater.*, 2018, **1**(2), 343.
14 L. Liang and P. Gao, *Adv. Sci.*, 2018, **5**(2), 1700331.
15 A. Kulkarni, T. Singh, M. Ikegami and T. Miyasaka, *RSC Adv.*, 2017, **7**, 9456.
16 T. Singh, A. Kulkarni, M. Ikegami and T. Miyasaka, *ACS Appl. Mater. Interfaces*, 2017, **8**(23), 14542.
17 B.-W. Park, B. Philippe, X. Zhang, H. Rensmo, G. Boschloo and E. M. J. Johansson, *Adv. Mater.*, 2016, **27**(43), 6806.
18 M. B. Johansson, H. Zhu and E. M. J. Johansson, *J. Phys. Chem. Lett.*, 2016, **7**(17), 3467.
19 C. N. Savory, A. Walsh and D. O. Scanlon, *ACS Energy Lett.*, 2016, **1**(5), 949.
20 Y. Kim, Z. Yang, A. Jain, O. Voznyy, G.-H. Kim, M. Liu, L. N. Quan, F. P. Garcia de Arquer, R. Comin, J. Z. Fan and E. H. Sargent, *Angew. Chem., Int. Ed.*, 2016, **55**(33), 9586.
21 H. Zhu, M. Pan, M. B. Johansson and E. M. J. Johansson, *ChemSusChem*, 2017, **10**(12), 2592.
22 Z. Shao, T. Le Mercier, M. B. Madec and Th. Pauporte, *Mater. Des.*, 2018, **141**, 81.
23 Z. Shao, T. L. Mercier, M. B. Madec and T. Pauporte, *Mater. Lett.*, 2018, **221**, 135.
24 M. Khazaee, K. Sardashti, J.-P. Sun, H. Zhou, C. Clegg, I. G. Hill, J. L. Jones, D. C. Lupascu and D. B. Mitzi, *Chem. Mater.*, 2018, **30**(10), 3538.
25 I. Turkevych, S. Kazaoui, E. Ito, T. Urano, K. Yamada, H. Tomiyasu, H. Yamagishi, M. Kondo and S. Aramaki, *ChemSusChem*, 2017, **10**, 3754.
26 X.-H. Zhu, N. Mercier, P. Frere, P. Blanchard, J. Roncali, M. Allain, C. Pasquier and A. Riou, *Inorg. Chem.*, 2003, **42**(17), 5330.
27 A. Kulkarni, T. Singh, A. K. Jena, P. Pinpithak, M. Ikegami and T. Miyasaka, *ACS Appl. Mater. Interfaces*, 2018, **10**(11), 9547.
28 K. W. Jung, M. R. Sohn, H. M. Lee, I. S. Yang, S. D. Sung, J. Kim, E. W.-G. Diau and W. I. Lee, *Sustainable Energy Fuels*, 2018, **2**, 294.
29 K. M. Boopathi, S. Raman, R. Mohanraman, F.-C. Chou, Y.-Y. Chen, C.-H. Lee, F.-C. Cheng and C.-W. Chu, *Sol. Energy Mater. Sol. Cells*, 2014, **121**, 35.

